UC Davis
UC Davis Previously Published Works

Title

Synergistic FRET assays for drug discovery targeting RyR2 channels

Permalink

https://escholarship.org/uc/item/2ps432rv

Authors

Rebbeck, RobynT

Ginsburg, Kenneth S

Ko, Christopher Y

et al.

Publication Date

2022-07-01

DOI

10.1016/j.yjmcc.2022.04.002

Peer reviewed

Synergistic FRET assays for drug discovery targeting RyR2 channels

Robyn T. Rebbeck[a], **Kenneth S. Ginsburg**[b], **Christopher Y. Ko**[b], **Anna Fasoli**[b], **Katherine Rusch**[a], **George F. Cai**[a], **Xiaoqiong Dong**[b], **David D. Thomas**[a,c], **Donald M. Bers**[b], **Razvan L. Cornea**[a,c,*]

[a]Department of Biochemistry, Molecular Biology and Biophysics, University of Minnesota, MN, USA

[b]Department of Pharmacology, University of California, Davis, CA, USA

[c]Photonic Pharma LLC, Minneapolis, MN, USA

Abstract

A key therapeutic target for heart failure and arrhythmia is the deleterious leak through sarcoplasmic reticulum (SR) ryanodine receptor 2 (RyR2) calcium release channels. We have previously developed methods to detect the pathologically leaky state of RyR2 in adult cardiomyocytes by monitoring RyR2 binding to either calmodulin (CaM) or a biosensor peptide (DPc10). Here, we test whether these complementary binding measurements are effective as high-throughput screening (HTS) assays to discover small molecules that target leaky RyR2. Using FRET, we developed and validated HTS procedures under conditions that mimic a pathological state, to screen the library of 1280 pharmaceutically active compounds (LOPAC) for modulators of RyR2 in cardiac SR membrane preparations. Complementary FRET assays with acceptor-labeled CaM and DPc10 were used for Hit prioritization based on the opposing binding properties of CaM vs. DPc10. This approach narrowed the Hit list to one compound, Ro 90–7501, which altered FRET to suggest increased RyR2-CaM binding and decreased DPc10 binding. Follow-up studies revealed that Ro 90–7501 does not detrimentally affect myocyte Ca^{2+} transients. Moreover, Ro 90–7501 partially inhibits overall Ca^{2+} leak, as assessed by Ca^{2+} sparks in permeabilized rat cardiomyocytes. Together, these results demonstrate (1) the effectiveness of our HTS approach where two complementary assays synergize for Hit ranking and (2) a drug discovery process that combines high-throughput, high-precision in vitro structural assays with in situ myocyte assays of

*Corresponding author at: Department of Biochemistry, Molecular Biology, and Biophysics, University of Minnesota, 6-155 Jackson Hall, 321 Church Street SE, Minneapolis, MN 55455, USA. corne002@umn.edu (R.L. Cornea).

the pathologic RyR2 leak. These provide a drug discovery platform compatible with large-scale HTS campaigns, to identify agents that inhibit RyR2 for therapeutic development.

Keywords

Calcium channel; RyR; Sarco/endoplasmic reticulum; Fluorescence lifetime; Calcium leak

1. Introduction

Cardiac muscle contraction is governed by Ca^{2+} release through ryanodine receptor type 2 calcium channels (RyR2) from the sarcoplasmic reticulum (SR), while relaxation requires RyR closure and active Ca^{2+} uptake into the SR by the SR Ca-ATPase (SERCA). Cytoplasmic Ca^{2+} is also critical for control of mitochondrial function, reactive oxygen species, and nuclear transcriptional signaling [1,2]. Elevated SR Ca^{2+} leak during diastole, via dysfunctional RyR2, contributes to elevated cytoplasmic $[Ca^{2+}]$ and reduced SR Ca^{2+} content, which are hallmarks of severe heart pathologies – heart failure (HF), arrhythmias, catecholaminergic polymorphic ventricular tachycardia (CPVT), and sepsis-associated cardiac dysfunction [3–5]. Furthermore, decreased SR Ca^{2+} content reduces the amount of SR Ca^{2+} released, which contributes to systolic dysfunction. There is strong evidence for the therapeutic potential of targeting RyR2 leak for treating HF and arrhythmias [6–9]. In particular, the therapeutic value of pharmaceutically targeting RyR2- mediated SR Ca^{2+} leak using dantrolene has been demonstrated for human HF cardiomyocytes and animal models of pulmonary arterial hypertension and ventricular tachycardia [9–12], and in a clinical trial targeting CPVT application [13].

Multiple mechanisms have been proposed to explain altered RyR2 gating that contributes to cardiomyopathies. In addition to CPVT-linked human RyR2 mutations, these include 1) RyR2 hyper-phosphorylation by protein kinase A (PKA) and its secondary FKBP12.6 dissociation [21], 2) RyR2 hyper-phosphorylation by calmodulin (CaM)-dependent protein kinase type II (CaMKII)- [22,23], 3) oxidation, which activates RyR2 directly [24–26] but also activates CaMKII [27], and 4) reduced RyR2/CaM binding [22,28] (Fig. 1A). The CPVT-linked mechanism is controversial [29–32], but the other four are well supported and accepted.

Using cardiomyocytes, we have developed structural assays of the patho-RyR2 state based on binding of RyR2 regulators CaM and a peptide that disrupts interdomain interactions (DPc10) [14,15]. We and others have observed an interplay of these modulators binding to RyR2. Specifically, reduced CaM affinity and increased DPc10 association typically reflect the hyperactive RyR2 resting state [15,19], which can be reversed by dantrolene [14,15] (Fig. 1A). We have shown that such measurements are scalable as structural assays for drug discovery via high-throughput screening (HTS), as previously established with RyR1-targeted assays [33,34]. These assays form the core of the novel platform we have developed to identify new small molecules that target RyR2 leak for HF and arrhythmia therapy.

We have recently validated the effectiveness of a screen that monitors CaM-RyR binding [33,34]. Although we did not observe a strict correlation between modulation of CaM binding to RyR1 and effect on RyR1 activity, we speculated that this rule may hold true for RyR2. With RyR2, we have the additional opportunity to develop a drug discovery process, initiated by concurrently running synergistic measurements of compound effects on CaM- and DPc10-RyR2 binding. As established with dantrolene in cardiomyocytes [14–16], we hypothesize that compounds with therapeutic potential will enhance CaM-RyR2 binding, and/or reduce DPc10-RyR2 binding, as shown in Fig. 1A. As with the effect of pathological conditions (H_2O_2, excess phosphorylation) in cardiomyocytes [16], we anticipate that compounds promoting RyR2 leak will reduce CaM binding and/or enhance DPc10 binding (Fig. 1A). It is difficult to predict the functional impact of a compound that alters CaM and DPc10 binding in the same direction. Based on our established CaM-RyR1 HTS-compatible platform [33,34], we are well positioned to use both assays for an orthogonal measurement of CaM-RyR2 and DPc10-RyR2 binding as a gauge of RyR2 modulators. Using these assays is a practical HTS strategy to discover modulators. It also tests further our working model (Fig. 1A), in which multiple pathological influences produce a common trilogy of states: reduced CaM affinity, increased DPc10 binding, and leaky RyR2, all of which can be remedied by dantrolene. Finding novel agents may be therapeutically beneficial, while enriching our understanding of CaM and DPc10 binding properties relative to SR Ca^{2+} leak.

Our HTS-compatible assay measures FLT to calculate FRET between an excited donor fluorophore attached to a single-Cys FKBP12.6 (D-FKBP) and an acceptor fluorophore attached to a single-Cys CaM (A-CaM) or N-terminus of DPc10 peptide (A-DPc10), when these labeled proteins bind to RyR2 in SR membranes (Fig. 1B). Shifts in FRET positively correlate with shifts in protein/peptide binding. In the present study, our goal is to validate this RyR2-focused HTS platform by screening a library of 1280 pharmacologically active compounds (LOPAC) for RyR2 modulators, using isolated cardiac SR preparations in diastolic conditions. Overall, the results demonstrate an early-stage screening process for RyR2-targeted drug discovery.

2. Materials and methods

2.1. Compound handling and preparation of 1536-well assay plates

The LOPAC compounds (Sigma-Aldrich, MO, USA) were received in 96-well plates and reformatted into assay plates as previously detailed [35,36]. Assay plates were prepared by transferring 5 nL of the 10 mM compound stocks in columns 3–22 and 27–46 or DMSO in columns 1–2, 23–26 and 47–48 from the source plates to 1536-well black polypropylene plates using an Echo 550 acoustic dispenser. These assay plates were stored at – 20 °C prior to usage.

2.2. Isolation of SR vesicles

Sarcoplasmic reticulum (SR) vesicles were isolated from porcine cardiac left ventricle tissue by differential centrifugation of homogenized tissue [37]. Vesicles were flash-frozen and stored at – 80 °C. Prior to the fluorescence assays described below, the SR vesicles were

stripped of residual endogenous CaM by incubation with a peptide derived from the CaM binding domain of myosin light chain kinase, followed by sedimentation [38].

2.3. Expression, purification and labelling of D-FKBP and A-CaM, and preparation of HL647-DPc10

Single-cysteine mutants of FKBP12.6 (C22A/T85C/C76I) and CaM (T34C) were expressed in *E. coli* BL21(DE3) pLysS (Agilent Technologies, CA, USA), purified, and respectively labeled, via thiol-maleimide reaction, with fluorescent probes AF488 or AF568, for D-FKBP and A-CaM, as described previously [39,40]. DPc10 peptides were synthesized and N-terminally labeled with HiLyte Fluor 647 (for A-DPc10) by AnaSpec (Fremont, CA) corresponding to the human RyR2 sequence 2459-GFCPDHKAAMVLFLDRVYGIEVQDFLLHLLEVGFLP-2494.

2.4. Preparation of SR vesicles for FRET measurements

Cardiac SR (1.5 mg/mL) membranes were treated with 100 μM H_2O_2 or water (control) for 1 h, at 21 °C, in binding buffer containing 150 mM KCl, 0.1 mg/mL BSA, 1 μg/mL Aprotinin/Leupeptin, and 20 mM PIPES (pH 7.0). SR was washed by centrifugation at 110,000 xg for 25 min and the pellet was resuspended to 1.6 mg/mL in binding buffer. Then, the SR was incubated with 60 nM D-FKBP for 90 min, at 37 °C, in binding buffer. To remove unbound D-FKBP, the SR membranes were spun down at 110,000 xg for 25 min, and then resuspended to 2 mg/mL in binding buffer, for a second spin and pellet resuspension (2 mg/mL in binding buffer). These samples were then incubated with 100 nM A-CaM or 1.5 μM A-DPc10, for 60 min, at 22 °C, in binding buffer containing 0.065 mM $CaCl_2$ to give 30 nM free Ca^{2+} in the presence of 1 mM EGTA (calculated by MaxChelator). The six separate SR samples included D-FKBP only, D-FKBP+A-CaM, and D-FKBP+A-DPc10, using SR with and without H_2O_2 pre-treatment. Each SR sample was applied to the assay plates in aliquots of 5 μL/well using a Multidrop™ Combi reagent dispenser (Thermo Fisher Scientific, MA, USA) with a long-tube metal-tip dispensing cassette (Thermo Scientific).

2.5. Fluorescence data acquisition

At 20 and 120 min after sample loading, fluorescence measurements were performed using high-throughput fluorescence plate-readers (Fluorescence Innovations, MN, USA) provided by Photonic Pharma LLC (MN, USA), including one detecting FLT and another detecting fluorescence spectra, as described previously [35,41–43].

2.6. HTS data analysis

Time-resolved fluorescence waveforms for each well were fitted based on a one-exponential decay function, using least-squares minimization global-analysis software, as detailed previously [42]. The FRET efficiency (*E*) was determined as the fractional decrease of donor FLT (τ_D), due to the presence of acceptor fluorophore (τ_{DA}), using the following equation:

$$E = 1 - \frac{\tau_{DA}}{\tau_D} \tag{1}$$

Typically, the statistics-based criterion for Hit selection is that it changes the result by >3SD. This is because the probability of a Hit being part of the normally-distributed control population is very small <0.3%, minimizing the probability of selecting false Hits. Here, a compound was selected as a Hit if it changed τ_{DA} by >4SD relative to control τ_{DA} (sample exposed to 0.1% DMSO).

2.7. [3H]Ryanodine binding to SR vesicles

In 96-well low-binding plates (Greiner Bio-One, Kremsmünster, Austria), 2 mg/mL cardiac SR vesicles were pre-incubated with 1% DMSO or Hit compound, with or without 100 μM H_2O_2, for 30 min at 22 °C in a solution containing 150 mM KCl, 1 μg/mL Aprotinin/Leupeptin, 1 mM EGTA, and 0.24 or 1.62 mM $CaCl_2$ (as determined by MaxChelator to yield 100 nM or 30 μM of free Ca^{2+}, respectively), 0.1 mg/mL BSA, 100 nM CaM, 5 mM sodium-adenosine triphosphate, and 20 mM K-PIPES (pH 7.0). Non-specific and maximal [3H]ryanodine binding to SR were separately assessed by addition of 40 μM non-radioactively labeled ryanodine or 5 mM adenylyl-imidodiphosphate and 20 mM caffeine, respectively. Such control samples were each distributed over 4 wells/plate. Binding of [3H]ryanodine (7.5 nM in each well) was determined after a 3-h incubation (37 °C) and filtration through grade GF/B Glass Microfiber filters (Brandel Inc., Gaithersburg, MD, US) using a 96-channel Brandel Harvester. In 4 mL of Ecolite Scintillation cocktail (MP biomedicals, Solon, OH, USA), [3H] retained on filter was counted using a Beckman LS6000 scintillation counter (Fullerton, CA, USA).

2.8. Cardiac ventricular myocyte isolation

Ventricular myocytes were isolated enzymatically from adult rabbit and rat hearts as previously described [44], and cells were used acutely (for additional details see Supplementary Methods). Each animal was anesthetized with isoflurane 2–5% to a verified deep surgical plane, whereupon the heart was excised, resulting in euthanasia by exsanguination. All animal handling and laboratory procedures were performed following a protocol approved by University of California Davis IACUC and conforming with AVMA and US PHS (Animal Welfare Act) guidelines.

2.9. Ca2+ transients and SR Ca2+ content in intact myocytes

We loaded myocytes with Fluo8-AM (green fluorescent calcium indicator, Abcam) at 5–6 μM for 25–27 min at room temperature, washing for an equal period to allow de-esterification. Myocytes were then transferred to normal Tyrode's solution composed of (in mM) 4 KCl, 140 NaCl, 1 $MgCl_2$, 5.5 glucose, 10 HEPES and either 2 (rabbit) or 1 mM $CaCl_2$ (rat) adjusted to pH 7.4 at room temperature. Cells were paced at 0.5 Hz, and we recorded Ca^{2+} transients (480 nM excitation, 530 nM detection), with a wide-field epifluorescence microscope and photometer, delimiting the detection field to one cell per experiment.

After an initial control pacing period (typically 5–10 min), we applied either Ro 90–7501 or piceatannol (10 μM, any given cell treated with only one drug) for an equal time, followed by washout. In all cells analyzed, fluorescence was stable during experiments, with only minor long-term trends, corrected as needed. During each treatment phase, pacing was

interrupted one or more times to record rest fluorescence, thus providing a stability check. With rabbit myocytes, pacing was stopped and caffeine was applied (10 mM, 8 s) once during each phase (Fig. 5B) to measure SR Ca^{2+} load.

Data acquisition and drug application/removal were computer-controlled, synchronous with pacing. Fluorescence was represented as $[Ca^{2+}]$ using a standard pseudo-ratio approach, after subtracting nonspecific background (additional details see Supplementary Methods). Ca^{2+} handling parameters were determined via built-in functions and home-written Visual Basic macros in Excel.

2.10. Ca^{2+} sparks and SR Ca^{2+} content in saponin-permeabilized myocytes

Freshly isolated rat ventricular myocytes were permeabilized with saponin (50 μg/ml) for 1 min in internal solution containing (in mM) 10 HEPES, 0.5 EGTA, 1 mM free $MgCl_2$ (with free $[Ca^{2+}]$ adjusted to 50 nM using MaxChelator), 120 K-aspartate, 10 reduced glutathione, 5 ATP, 5 phosphocreatine di-Na, creatine phosphokinase 5 U/mL, and dextran (MW: 40,000) 4% at pH 7.2. Myocytes were immediately washed with saponin-free internal solution and then superfused with internal solution containing 10 μM Fluo-4 pentapotassium salt (Invitrogen™, Thermofisher Scientific) for Ca^{2+} fluorescence imaging. Ca^{2+} sparks were recorded on a confocal microscope (Bio-Rad, Radiance 2100, 40× objective) in line scan mode (166 lines/s; ex 488 nm, em >505 nm). Only healthy permeabilized myocytes with no ultrastructural damage and exhibiting consistent spark activity without wave events were selected for data acquisition. The pathologically leaky conformation of RyR2 was promoted by incubating myocytes for 1 h with 50 μM H_2O_2 in normal Tyrode's solution before permeabilizing. Ca^{2+} sparks and RyR2 activity were also assessed after incubating permeabilized myocytes for 5 min with 10 μM Ro 90–7501 or 500 μM tetracaine. Ca^{2+} sparks were detected and analyzed using the SparkMaster plugin for ImageJ [45]. The Criteria parameter was set to 3.8 SD above baseline as default and adjusted incrementally until false-positive and false-negative spark detections were minimized. The colour display scale for representative Ca^{2+} spark linescan images was adjusted to span the fluorescence range of Ca^{2+} sparks. The green saturation point was set to a fluorescence value that is 10% above the fluorescence of the brightest spark (excluding outliers) relative to the baseline Ca^{2+} signal fluorescence, which was calculated as: median fluorescence +110% (fluorescence of pixel of 99.99th percentile brightness - median fluorescence). SR Ca^{2+} load was determined by evaluating the amplitude of the Ca^{2+} fluorescence signal (normalized to the baseline diastolic fluorescence, F_0) induced by rapid localized delivery of 10 mM caffeine. Chemical reagents were purchased from Sigma-Aldrich unless indicated otherwise.

2.11. Analysis and presentation of data

Data are presented as mean ± SD or ± SEM, as indicated. For statistical difference determination, we used paired Student's *t*-test or unpaired Student's t-test, as indicated. Statistical analyses were performed with GraphPad Prism 9 or Origin, as indicated. Significance was accepted at $P < 0.05$.

3.   Results

3.1.   HTS performance

To test the performance of our FRET assays (FRET between D-FKBP and A-CaM, and between D-FKBP and A-DPc10), we screened the 1280-compound LOPAC in 1536-well plates. Each well of this assay plate was pre-loaded with 5 nL of compound (10 mM in DMSO for 10 μM final concentration) or DMSO (control over 256 wells). Prior to preparing the compound plates, each FRET assay involved incubating D-FKBP-labeled SR membranes with sub-saturating A-CaM (150 nM) or A-DPc10 (1.5 μM). The use of sub-saturating concentrations was designed to enable sensitivity for compounds that increased or decreased acceptor-labeled protein binding to RyR2. Final assay conditions also included 30 nM Ca^{2+} to represent diastolic $[Ca^{2+}]$. To test whether compound effect could be impacted by healthy vs. pathological state of RyR2, we pre-incubated the SR with and without H_2O_2 prior to labelling with fluorescent proteins. The pre-incubation specifically promoted the pathological state of RyR2, while minimizing the additional complication of oxidizing CaM and DPc10.

FRET values were calculated from lifetimes determined from fluorescence decay waveforms acquired 20 and 120 min after loading SR samples to the assay plates. Fluorescently interfering compounds were identified when the corresponding donor-only lifetime was altered by >3SD of the DMSO mean, and/or the fluorescence spectrum of the unlabelled SR was altered by >3SD, as previously described [33,34]. These interfering compounds were removed from further consideration. For both A-CaM and A-DPc10 FRET, the number of Hits trended to be greater with the longer (120 min) incubation (Table 1 and Supplementary Table 1), aligning with previous RyR1-targeted FRET screens [33,34]. Correspondingly, remaining FRET results are reporting on the 120 min incubation result.

As shown in Fig. 2, compound effects can be directly compared between A-CaM and A-DPc10 FRET. Compound effects beyond SD thresholds can be separated into 8 sectors (denoted by cardinal points) based on North-South and East-West coordinates, where SE sector would be most desirable for Hits that enhance CaM binding and reduce DPc10 binding. Compounds that alter both FRET values in the same direction (sector SW or NE) are potentially altering FKBP binding rather than both A-CaM and A-DPc10. This is most evident by temsirolimus, previously shown to alter D-FKBP binding to RyR1 and 2 [34], in sector SW (Fig. 2). Compounds in sections other than SW and NE are more likely to alter binding of A-CaM and/or DPc10, with the effect on FRET correlating with protein binding. Suramin appeared in sector W (Fig. 2), consistent with its well-established role in dissociating fluorescently labeled CaM from RyRs [20].

Regardless of sector effect, the Hit rate was similar between no-H_2O_2 and H_2O_2 treatment plates for both A-CaM and A-DPc10 FRET (Table 1 and Supplementary Table 1). Acceptable hit rates for HTS assays range ~ 0.5 to 3%, in order to yield a manageable load of post-HTS testing via secondary assays [46]. Application of this selection criterion meant that a threshold of 4SD would be suitable for our HTS assays, yielding $2.7 \pm 1.1\%$ and $4.8 \pm 2.1\%$ hit rates for the A-DPc10 and A-CaM assays, respectively (Table 1). Of key

importance, using a 4SD threshold, Hit reproducibility between 2 of 3 screen replicates was only slightly higher than reproducibility between all 3 screen replicates (Table 1).

As shown in Fig. 3, the effect on FRET was reproducible for the three screen replicates. Focusing on compounds identified as Hits in at least 2 of the 3 screen replicates, 18 compounds were Hits in both A-CaM and A-DPc10 FRET, while 19 and 5 compounds were Hits in only A-CaM or A-DPc10 FRET, respectively (Fig. 3). Compound effects were very similar between 0 and 100 μM H_2O_2 treatment for both A-CaM and A-DPc10 FRET. However, most compounds altered A-CaM and A-DPc10 FRET differently, with the exception of temsirolimus (Fig. 3), which alters D-FKBP binding [34]. Between these RyR2 screens and our previous LOPAC RyR1-targeted screen using D-FKBP and A-CaM, we similarly detected aurintricarboxylic acid (ATA), benserazide, diltiazem, temsirolimus, 6-hydroxyl DL-DOPA, NF 023, Myricetin, Ro 90–7501, cisplatin, aurothioglucose, reactive blue 2, SCH-202676, disulfiram, suramin, N-propylnorapomorphine (R(−)-NPA), and IPA-3 [34]. Though, benserazide and 6-hydroxy-DL-DOPA were detected only by the A-DPc10, rather than A-CaM, FRET assay (Fig. 3). We were pleased to re-identify these Hits, several of which being known RyR modulators. Specifically, diltiazem, suramin, NF023 and disulfiram have been previously shown to increase RyR1/2 activity, and ATA, myricetin and Ro 90–7501 have been shown to decrease RyR1/2 activity [33,34,47]. We also identified known RyR modulators beyond those identified in our RyR1 LOPAC screen, including amsacrine [48] and S-nitrosoglutathione [49,50]. Although known to not alter RyR1 activity, catechin has an analogue that is known to increase RyR1 and 2 activity [51,52].

Several Hits are known to bind directly to CaM or FKBP, or alter binding of these modulators to RyR. Indeed, suramin is commonly used as a control to strip CaM from RyR1/2 in our FRET assays [20]. Unsurprisingly, a suramin analogue, NF 023, also reduced A-CaM FRET (Fig. 3A). S-nitrosoglutathione has been shown to reduce CaM and FKBP12.0 binding to RyR1 [53], which aligns with the observed decrease in A-CaM FRET (Fig. 3A). We have previously shown that temsirolimus greatly reduces FKBP12.6 binding to RyR2 [34], which strongly agrees with its decrease of both A-CaM and A-DPc10 FRET (Figs. 2 and 3). Both droperidol and 6-hydroxymelatonin have been found to bind to CaM [54,55]. Cisplatin has been shown to mediate CaM crosslinking [56].

In sector NW (compounds that increase A-DPc10 FRET and decrease A-CaM FRET) we identified 10 reproducible Hits (Fig. 3), including two compounds (NF 023 and disulfiram) that are known to increase RyR1/2 activity [33,47]. Conversely, Ro 90–7501, the one reproducible Hit in sector SE that reduced A-DPc10 FRET and increased A-CaM FRET, has been shown to decrease RyR1 and 2 activity [34]. This finding supports our hypothesis that CaM and DPc10 binding reflects RyR2 functional state (Fig. 1). Consistent with this hypothesis, amsacrine in sector E (increased A-CaM FRET) has been implicated in reducing RyR1 leak [48]. Furthermore, suramin and S-nitrosoglutathione in sector W (decreased A-CaM FRET), have been found to increase RyR1 and 2 activity [47,49,50]. Notably, ATA in sector W (Fig. 3) complicates our hypothesis, as we previously demonstrated that ATA reduces RyR2 activity in nM [Ca^{2+}] [34].

Of the six Hits in sector NE that increased both A-CaM and A-DPc10 FRET, myricetin reduced RyR1 and RyR2 activity in nM $[Ca^{2+}]$, which suggests that this sector may also contain compounds of therapeutic interest. To investigate further, we purchased 11 Hits and assessed the dose response for the FRET and RyR2 activity assays, with particular focus on the sole Hit in the SE sector, Ro 90–7501.

3.2. FRET dose-response assay

Using the same FRET assays (A-CaM and A-DPc10) as in HTS, in "healthy" and "pathological" conditions (0 and 100 μM H_2O_2 pre-treatment, respectively), we tested the dose response for key Hits from these screens. The FRET dose-response assays of LOPAC Hits largely replicated the effect found in the primary screens (Fig. 4A, Supplementary Fig. 4). All compounds altered both A-CaM and A-DPc10 FRET, including compounds that only altered A-CaM FRET (specifically ATA, reserpine and suramin) or A-DPc10 FRET (specifically MRS 2159) in the primary screens (Figs. 3, 4A, Supplementary Fig. 4). Notably, most of these new effects are subtle, and would not exceed the 4SD threshold of the primary screen. This is a manifestation of the imperfect reproducibility between the compounds in the libraries and repurchased, which is a routine problem in HTS.

Replicating the effect of 10 μM compound in the primary screening (Fig. 3), micromolar Ro 90–7501 increased A-CaM FRET and decreased A-DPc10 FRET (Fig. 4A). We previously reported the inhibitory effect of Ro 90–7501 RyR1 and 2 [34]. With the FRET profile of decreasing A-DPc10 FRET and increasing A-CaM FRET, the inhibitory effect of Ro 90–7501 aligns with the hypothesis in Fig. 1.

Of the 11 purchased compounds, 5 compounds (cisplatin, disulfiram, IPA-3, SCH-202676 and suramin) displayed a similar FRET dose response profile – largely decreasing A-CaM FRET and with a biphasic effect on A-DPc10 FRET (Supplementary Fig. 4). Curiously, the effect of piceatannol, strongly increasing both A-CaM and A-DPc10 FRET, is very similar to that of myricetin (Supplementary Fig. 4). With myricetin previously demonstrated to decrease RyR2 activity, perhaps piceatannol may as well. This may also hold true for other compounds (e.g., MRS 2159 and reserpine) that increase A-CaM and A-DPc10 FRET (Supplementary Fig. 4), though to a lower degree relative to myricetin. These features highlight a new category for further studies, which is the functional state of RyR2 characterized by both increased CaM and DPc10 binding.

3.3. Effect of hits on RyR activity using [³H]ryanodine binding assays

To evaluate the functional impact of compounds identified through our FRET-based screen, we first used [³H]ryanodine binding assays. The level of [³H]ryanodine binding to RyRs in SR membranes is a well- established index of RyR channel activity [40]. At 0.1 and 30 μM Ca^{2+}, low micromolar Ro 90–7501 decreased RyR2 activity by 10% (Fig. 4B), which aligns with our previous report of Ro 90–7501 decreasing RyR2 activity in nanomolar Ca^{2+} [34].

At 100 nM Ca^{2+}, 1–10 μM piceatannol reduced RyR2 activity by up to 56%, and >30 μM increased RyR2 activity (Supplementary Fig. 5B). In contrast, >10 μM piceatannol only increased RyR2 activity at 30 μM Ca^{2+} (Supplementary Fig. 5B). Curiously, reserpine,

another compound that increased both A-CaM and A-DPc10 FRET, only increased RyR2 activity at 100 nM Ca^{2+} (Supplementary Fig. 5C).

With similar FRET effects, cisplatin and SCH 202676 both decrease RyR2 activity at 100 nM Ca^{2+} and increase RyR2 activity at 30 μM Ca^{2+} (Supplementary Fig. 5A and B). However, higher concentrations led to divergent biphasic effects, with >30 μM cisplatin increasing activity at 100 nM Ca^{2+}, and 100 μM SCH 202676 decreasing activity at 30 μM Ca^{2+} (Supplementary Fig. 5A and D). Biphasic dose-response curves are often observed in biology, and particularly in pharmacology (a behavior termed hormesis [57]).

3.4. Ro 90–7501 does not affect Ca^{2+} transients in adult ventricular myocytes

Initial myocyte safety tests for these potential RyR conformational modulator Hits were to assess for any negative effects on normal cardiac myocyte function. Ro 90–7501 (10 μM) had no major effect on overall Ca^{2+} handling properties of normal rabbit myocytes (Fig. 5). Fig. 5A displays a (decimated) time series recording of an entire experiment, showing cytosolic $[Ca^{2+}]$ ($[Ca^{2+}]_i$) responses to trains of pacing stimuli (0.5 Hz, 40 s each), exposure to Ro 90–7501 (10 μM), and discrete applications of caffeine (10 mM, 8 s). Baseline diastolic $[Ca^{2+}]_i$ was assumed to be at 100 nM for these pseudo-ratiometric fluorescence measurements, and red dots mark 30-s rest periods in which $[Ca^{2+}]_i$ returns to baseline were ensured. Transient perturbations to the steady state were due to rest periods or caffeine-induced SR Ca^{2+} depletion (indicated in Fig. 5B). Fig. 5B shows steady state twitch Ca^{2+} transients, followed by caffeine responses to assess SR Ca^{2+} content, including the first 2–4 beats after caffeine removal during control (left), drug (middle) and washout (right) periods. Fig. 5C-G show average values for peak $[Ca^{2+}]_i$, time constant (τ) of twitch Ca^{2+} transient decay, diastolic $[Ca^{2+}]_i$ (predicted by fits to the $[Ca^{2+}]_i$ decline phase), SR Ca^{2+} load and τ of caffeine-induced Ca^{2+} transient decay (an assay of mainly Na/Ca exchanger function [44]). Parameters shown were unaffected or only mildly affected. This mild effect of 10 μM Ro 90–7501 on Ca^{2+} transient amplitude is consistent with its minimal functional effect on [^{3}H]ryanodine binding at 30 μM Ca^{2+} (Fig. 4B). This minimal effect was also observed for piceatannol, which did not alter RyR2 activity in SR vesicles, and had minimal effects on Ca^{2+} transients in cardiomyocytes (Supplementary Fig. 6). It is important to note that numerical significances were small, and only present when t-tests were paired (as denoted by asterisks). Therefore, we consider these small differences to be of minimal physiological significance, although the slight acceleration of Ca^{2+} transient decay with both Ro 90–7501 and piceatannol would be in the direction expected for a drug that limits SR Ca^{2+} leak (Fig. 5D, Supplementary Fig. 6).

Ro 90–7501 or piceatannol effects were also insignificant or minimal in rat. Ca^{2+} transient time to peak (not shown) was unaffected by Ro 90–7501 or piceatannol in either rabbit or rat myocytes. This aligns with a previous study demonstrating 10 μM piceatannol has insignificant effects on Ca^{2+} transients in rat cardiomyocyte [58].

We also examined extensive time series data (example in Fig. 5A) for possible short-lived effects at times of drug application/removal, which might have revealed short-term autoregulatory effects [59], but such effects were not seen consistently, and disappeared when time-aligned and averaged (40–50 transitions of each type examined) (Fig. 5C). Thus,

neither Ro 90–7501 nor piceatannol produced substantive transient or steady state effects on rabbit ventricular myocyte Ca^{2+} transients. We performed similar experiments in adult rat ventricular myocytes (not shown), and again saw no effects of either Ro90–7501 or piceatannol. Thus, for intact myocyte Ca^{2+} transients, neither agent produced observable negative effects.

3.5. Ro 90–7501 lowers Ca^{2+} spark rate in permeabilized rat myocytes

Ro 90–7501 had the best profile with respect to enhancing CaM binding and limiting DPc10 access, making it the higher priority compound to test for suppression of diastolic SR Ca^{2+} leak. For this reason we tested whether Ro 90–7501 inhibits SR Ca^{2+} leak in adult cardiomyocytes. We measured Ca^{2+} sparks in saponin-permeabilized rat ventricular myocytes using 6 s linescan images over a 5 min timeframe (at 0, 1, 3, and 5 min) to limit photobleach and phototoxicity. Paired recordings (Fig. 6A) and timecourse measurements (Fig. 6B) show that Ca^{2+} spark frequency (CaSpF) at control (Ctrl) baseline was stable over the 5 min period observed. Fig. 6B shows that Ro 90–7501 (10 μM) treatment reduced CaSpF, mostly over the first minute, and stabilized over 5 min at a lower level ($P = 0.041$, F = 3.00, time × treatment interaction effect). Fig. 6C shows a larger cohort of paired Ca^{2+} spark measurements after 5 min exposure to Ro 90–7501 either in Ctrl conditions or after pretreatment with 50 μM H$_2$O$_2$ prior to permeabilization [15]. As expected, H$_2$O$_2$ increased CaSpF, but Ro 90–7501 significantly reduced CaSpF in both Ctrl and H$_2$O$_2$-treated myocytes, as did 500 μM tetracaine, which submaximally inhibits Ca^{2+} sparks (Fig. 6C). Fig. 6D shows that Ro 90–7501, H$_2$O$_2$ and tetracaine all significantly altered CaSpF (in an unpaired analysis). Fig. 6E shows average Ca^{2+} spark characteristics and SR Ca^{2+} load, relevant because CaSpF strongly depends on, and also influences, SR Ca^{2+} content. That is, Ro 90–7501 reduced Ca^{2+} spark frequency and amplitude, resulting in a tendency to increase SR Ca^{2+} load (mimicking tetracaine, as a positive control for block of SR Ca^{2+} leak). H$_2$O$_2$ produced the opposite effects – increased spark frequency and amplitude – resulting in a major reduction of SR Ca^{2+} load. But in this H$_2$O$_2$-induced pathological RyR2 setting, Ro 90–7501 reduced CaSpF, amplitude and enhanced SR Ca^{2+} load.

A primary increase in CaSpF (as with H$_2$O$_2$) should reduce SR Ca^{2+} load, so reduction should by itself reduce CaSpF, thereby intrinsically limiting the extent of increase in CaSpF [60]. Thus, the ability of Ro 90–7501 to inhibit SR Ca^{2+} leak is underestimated by the reduced CaSpF per se, because the higher SR Ca^{2+} load itself partly offsets that suppression.

4. Discussion

This study implements the first high-throughput drug discovery process specifically aimed at RyR2 dysfunction, which has been linked to major clinical indications in cardiology and neurodegeneration. For HTS, we used two complementary FRET assays based on the working hypothesis that CaM and DPc10 binding to RyR2 identify allosteric small-molecule modulators of Ca^{2+} release through RyR2 (Fig. 1). In screening the 1280-compound LOPAC collection, we identified drug-like small-molecules that altered the A-CaM and/or A-DPc10 FRET measurements. Of potential therapeutic interest for increasing A-CaM FRET and decreasing A-DPc10 FRET, we identified Ro 90–7501 as an RyR inhibitor.

Using [³H]ryanodine-binding assays, we found several other Hits that are previously unknown functional modulators of RyR2. By demonstrating the mitigating effects of Ro 90–7501 on SR Ca^{2+} leak in adult cardiomyocytes, we validated the effectiveness of using complementary assays in our HTS platform.

Our working hypothesis – that the functional impact of RyR allosteric modulators may be identified through monitoring CaM and DPc10 binding to RyR2 (Fig. 1) – is based primarily on cardiomyocyte studies showing that CaM-RyR2 binding positively correlates with RyR2 healthy state, while DPc10-RyR2 binding negatively correlates with that same state [14]. The strongest evidence from our study supporting this hypothesis is that the combined structural results placing Ro 90–7501 in sector SE (decrease A-DPc10 FRET, increase A-CaM FRET) correlate with decreased pathological SR Ca^{2+} leak in adult cardiomyocytes, with minimal effects on healthy excitation-contraction coupling (Figs. 2, 3, 5 and 6). In the opposite sector (NW), with compounds that decrease A-CaM and increase A-DPc10, we identified compounds known to activate RyR1, including NF 023 and disulfiram [33,47]. However, upon further testing of other compounds in this sector, we found that cisplatin has biphasic effects and micromolar SCH-202676 reduces RyR2 activity (Supplementary Fig. 5). Thus, the counter-hypothesis does not quite hold true, that all compounds decreasing A-CaM FRET and increasing A-DPc10 FRET also increase RyR2 leak.

In sector NE (increased A-CaM and A-DPc10 FRET), myricetin [34] and 1–10 μM piceatannol decrease RyR2 activity. Notably, reserpine was found to slightly increase both FRET measurements in follow-up dose-response studies, and this compound slightly increases RyR2 activity. This suggests that compounds with FRET dose-response profiles similar to myricetin and piceatannol (in the NE sector of Fig. 2) may have greater therapeutic potential than more subtle modulators, such as reserpine (in the E sector). In future research, we plan to focus in more detail on the functional impact of NE compounds in parallel with other compounds that will be identified by screening larger chemical libraries.

Prior to this RyR2 screen, two RyR1-targeted HTS-compatible screens have been reported. We have reported a similar A-CaM FRET assay using skeletal SR (RyR1 isoform), rather than the cardiac SR used here (RyR2) [33,34]. In those RyR1 screens, we have identified 17 Hits: ATA, benserazide, diltiazem, temsirolimus, 6-hydroxyl DL-DOPA, NF 023, myricetin, Ro 90–7501, cisplatin, aurothioglucose, reactive blue 2, SCH-202676, disulfiram, suramin, R(−)-NPA, and IPA-3 [34]. Only four of these previously identified RyR1 Hits were not identified as Hits in the present RyR2-targeted FRET assays. This suggests isoform selectivity.

In 2018, Murayama and colleagues reported a complementary HTS assay that measures ER Ca^{2+} in mammalian cells recombinantly expressing WT and mutant RyR1 (associated with malignant hyperthermia) [48,61]. The Hits from their 1535-compound library are also present in the library we used here, including oxolinic acid, cinoxacin, lomefloxacin, ofloxacin, amsacrine and phenyl biguanide [48]. Of these, cinoxacin, lomefloxacin, and ofloxacin also altered our RyR2 FRET assays at the 3SD threshold, i.e., they would be Hits with a less stringent selection. Furthermore, we identified amsacrine in sector E, with

an increase in A-CaM binding (Fig. 3), aligning with the previous finding of amsacrine increasing ER Ca^{2+} in cells expressing WT RyR1 [48]. Consistent with a lack of effect on ER Ca^{2+} in mammalian cells expressing RyR2 [62], our RyR2 FRET assays did not pick up oxolinic acid on our HTS runs here.

The strength of Murayama's in-cell phenotypic HTS-compatible assay is that it provides immediate functional RyR validation in HEK cells. Indeed, that assay may pick up Hits that block or inhibit RyR function in multiple ways (including by orthosteric occlusion of the channel pore). In contrast, our primary FRET assays provide two separate allosteric measurements of a specific pathologically leaky RyR2 conformation that exhibits both reduced CaM-binding and enhanced DPc10 binding (in heart failure, oxidative stress, CPVT and CaMKII-dependent phosphorylation) [14,15,19,63]. While this does require follow-up tests in adult ventricular myocytes for functional validation, our conformational modulation approach is a strength of our strategy. That is because our Hits may allosterically shift the leaky diastolic RyR2 conformation back toward the normal healthy conformation without inhibiting physiological SR Ca^{2+} release during excitation-contraction coupling (as may occur with an orthosteric RyR2 modulator, aka blocker). Furthermore, a major strength of our FRET strategy is that our primary measurement is the direct response of target engagement with RyR2 or a regulator (FKBP, CaM or DPc10). Finally, our assays are carried out in 1536-well plates (vs. 96-well plates [48,61]) that are read in <6 min, a format that is compatible with industrial-scale screening setups.

Other approaches to RyR-targeted screening can be contemplated, e. g., by using biosensor systems that can be expressed for HTS in live cells, as we have demonstrated with SERCA and phospholamban [64,65]. For RyR2, prime candidates for this approach would be intra- and inter- protomeric FRET constructs similar to those engineered by Chen and collaborators [66,67]. The FLT plate reader we used for this study is ideally suitable to measure such samples. However, an important requirement for this approach is abundant expression of the engineered RyR in a cell line compatible with large-scale culture. This approach would provide important advantages, e.g., ability to use human RyR2 and include pathology-linked mutations. Different biosensor architectures will inherently yield different Hit sets from screening the same library, thus expanding the range of compounds of interest.

Immediate future work with the current HTS platform involves screening larger (50,000-compound) libraries, followed by lead development after functional validation (Fig. 7). We were somewhat taken aback by variability in the number of Hits per run, until we looked further into the consistency of compound effects for reproducible Hits (4SD threshold in 2 of 3 screens). Given that we observed consistency between the FRET effects of primary Hits and the FRET and functional effects of the repurchased Hits, we could also move forward with a duplicate screen and a less stringent threshold (e.g., 3SD) to identify the more subtle reproducible modulators. A key component of future functional testing will involve using myocytes from healthy and pathological models. Currently, testing compound effects on Ca^{2+} transient and SR Ca^{2+} leak remains an ultra-low throughput process. However, with increased throughput capabilities, HTS Hit compounds can be effectively tested using patient-derived human-induced pluripotent stem cell-derived cardiomyocytes (hiPSC-CMs) [68,69]. As shown in the Fig. 7 screening funnel, hiPSC-CMs will represent an important

component in hit-to-lead development from compounds identified via HTS of larger small-molecule libraries with diverse chemical scaffolds.

In summary, we have described an approach with high potential for early-stage RyR2-targeted drug discovery, demonstrating that our HTS-compatible assays identify compounds that decrease RyR2 Ca^{2+} leak, as confirmed using [^{3}H]ryanodine binding assays and SR Ca^{2+} leak in adult cardiomyocytes. The potential significance of this project reaches well beyond HF, as RyR Ca^{2+} leak is a key defect in several other pathologies, e.g., Alzheimer's and other age-related neurological diseases [70,71]. Beyond the primary translational impact of these screening projects, the newly identified RyR modulators may be used as tools for testing hypotheses of structure-function correlations, which will feed back to inform their mechanism of action and the structural pathways involved in the allosteric regulation of RyRs.

Supplementary Material

Refer to Web version on PubMed Central for supplementary material.

Acknowledgements

Abbreviations:

7,8-DHF	7,8-Dihydroxyflavone hydrate
A-CaM	acceptor labeled calmodulin
A-DPc10	acceptor labeled DPc10
AET	2-(2-Aminoethyl)isothiourea dihydrobromide
APDC	Ammonium pyrrolidinedithiocarbamate
BSA	bovine serum albumin
CaMKII	Calcium/calmodulin-dependent protein kinase II
CaT	calcium transient
cDPCP	cis-diammine(pyridine)chloroplatinum(II) chloride
CPVT	catecholaminergic polymorphic ventricular tachycardia
Ctrl	control
D-FKBP	donor-labeled FK506 binding protein 12.6

DMPP	1,1-dimethyl-4-phenylpiperazinium iodide
E	FRET efficiency
E	east
EGTA	ethylene glycol-bis(β-aminoethyl ether)-N,N,N′,N′-tetra-acetic acid
FLT	fluorescence lifetime
HEPES	4-(2-hydroxyethyl)-1-piperazineethanesulfonic acid
HTS	high-throughput screening
LOPAC	library of pharmacologically active compounds
N	North
NOBP	6-nitroso-1,2-benzopyrone
Pice	piceatannol
PIPES	piperazine-N,N′-bis(2-ethanesulfonic acid)
PKA	protein kinase A
R(−)-2-OH-Npa HBr	R(−)-2,10,11-trihydroxy-N-propylnoraporphine hydrobromide
R(−)-NPA	N-propylnorapomorphine
Ro90	Ro 90–7501
RyR	ryanodine receptor
S	south
SR	sarcoplasmic reticulum
SERCA	sarco/endoplasmic reticulum Ca-ATPase
W	west

References

[1]. Bers DM, Cardiac excitation-contraction coupling, Nature 415 (6868) (2002) 198–205. [PubMed: 11805843]

[2]. Bers DM, Calcium cycling and signaling in cardiac myocytes, Annu. Rev. Physiol. 70 (2008) 23–49. [PubMed: 17988210]

[3]. Kho C, Lee A, Hajjar RJ, Altered sarcoplasmic reticulum calcium cycling–targets for heart failure therapy, Nat. Rev. Cardiol. 9 (12) (2012) 717–733. [PubMed: 23090087]

[4]. Efremov RG, Leitner A, Aebersold R, Raunser S, Architecture and conformational switch mechanism of the ryanodine receptor, Nature 517 (7532) (2015) 39–43. [PubMed: 25470059]

[5]. Sepulveda M, Gonano LA, Viotti M, Morell M, Blanco P, Alarcon ML, Ramos IP, Carvalho AB, Medei E, Vila Petroff M, Calcium/calmodulin protein kinase II-dependent ryanodine receptor phosphorylation mediates cardiac contractile dysfunction associated with sepsis, Crit. Care Med. 45 (5) (2017) e399–e408. [PubMed: 27648519]

[6]. McCauley MD, Wehrens XH, Targeting ryanodine receptors for anti-arrhythmic therapy, Acta Pharmacol. Sin. 32 (6) (2011) 749–757. [PubMed: 21642946]

[7]. Roe AT, Frisk M, Louch WE, Targeting cardiomyocyte Ca2+ homeostasis in heart failure, Curr. Pharm. Des. 21 (4) (2015) 431–448. [PubMed: 25483944]

[8]. Bers DM, Stabilizing ryanodine receptor gating quiets arrhythmogenic events in human heart failure and atrial fibrillation, Heart Rhythm. 14 (3) (2017) 420–421. [PubMed: 27725286]

[9]. Hartmann N, Pabel S, Herting J, Schatter F, Renner A, Gummert J, Schotola H, Danner BC, Maier LS, Frey N, Hasenfuss G, Fischer TH, Sossalla S, Antiarrhythmic effects of dantrolene in human diseased cardiomyocytes, Heart Rhythm. 14 (3) (2017) 412–419. [PubMed: 27650424]

[10]. Huang Y, Lei C, Xie W, Yan L, Wang Y, Yuan S, Wang J, Zhao Y, Wang Z, Yang X, Qin X, Fang Q, Fang L, Guo X, Oxidation of ryanodine receptors promotes Ca(2+) leakage and contributes to right ventricular dysfunction in pulmonary hypertension, Hypertension 77 (1) (2021) 59–71. [PubMed: 33249863]

[11]. Kajii T, Kobayashi S, Shiba S, Fujii S, Tamitani M, Kohno M, Nakamura Y, Nanno T, Kato T, Okuda S, Uchinoumi H, Oda T, Yamamoto T, Yano M, Dantrolene prevents ventricular tachycardia by stabilizing the ryanodine receptor in pressure- overload induced failing hearts, Biochem. Biophys. Res. Commun. 521 (1) (2020) 57–63. [PubMed: 31635807]

[12]. Kryshtal DO, Blackwell DJ, Egly CL, Smith AN, Batiste SM, Johnston JN, Laver DR, Knollmann BC, RYR2 channel inhibition is the principal mechanism of flecainide action in CPVT, Circ. Res. 128 (3) (2021) 321–331. [PubMed: 33297863]

[13]. Penttinen K, Swan H, Vanninen S, Paavola J, Lahtinen AM, Kontula K, Aalto-Setala K, Antiarrhythmic effects of dantrolene in patients with catecholaminergic polymorphic ventricular tachycardia and replication of the responses using iPSC models, PLoS One 10 (5) (2015), e0125366.

[14]. Uchinoumi H, Yang Y, Oda T, Li N, Alsina KM, Puglisi JL, Chen-Izu Y, Cornea RL, Wehrens XH, Bers DM, CaMKII-dependent phosphorylation of RyR2 promotes targetable pathological RyR2 conformational shift, J. Mol. Cell. Cardiol. 98 (2016) 62–72. [PubMed: 27318036]

[15]. Oda T, Yang Y, Uchinoumi H, Thomas DD, Chen-Izu Y, Kato T, Yamamoto T, Yano M, Cornea RL, Bers DM, Oxidation of ryanodine receptor (RyR) and calmodulin enhance Ca release and pathologically alter, RyR structure and calmodulin affinity, J. Mol. Cell. Cardiol. 85 (2015) 240–248. [PubMed: 26092277]

[16]. Sufu-Shimizu Y, Okuda S, Kato T, Nishimura S, Uchinoumi H, Oda T, Kobayashi S, Yamamoto T, Yano M, Stabilizing cardiac ryanodine receptor prevents the development of cardiac dysfunction and lethal arrhythmia in Ca(2+)/calmodulin-dependent protein kinase IIdeltac transgenic mice, Biochem. Biophys. Res. Commun. 524 (2) (2020) 431–438. [PubMed: 32007269]

[17]. Rebbeck RT, Nitu FR, Rohde D, Most P, Bers DM, Thomas DD, Cornea RL, S100A1 protein does not compete with calmodulin for ryanodine receptor binding but structurally alters the ryanodine receptor, Calmodulin Complex J. Biol. Chem. 291 (30) (2016) 15896–15907.

[18]. Walweel K, Gomez-Hurtado N, Rebbeck RT, Oo YW, Beard NA, Molenaar P, Dos Remedios C, van Helden DF, Cornea RL, Knollmann BC, Laver DR, Calmodulin inhibition of human RyR2 channels requires phosphorylation of RyR2-S2808 or RyR2-S2814, J. Mol. Cell. Cardiol. 130 (2019) 96–106. [PubMed: 30928430]

[19]. Oda T, Yang Y, Nitu FR, Svensson B, Lu X, Fruen BR, Cornea RL, Bers DM, In cardiomyocytes, binding of unzipping peptide activates ryanodine receptor 2 and reciprocally inhibits calmodulin binding, Circ. Res. 112 (3) (2013) 487–497. [PubMed: 23233753]

[20]. Guo T, Fruen BR, Nitu FR, Nguyen TD, Yang Y, Cornea RL, Bers DM, FRET detection of calmodulin binding to the cardiac RyR2 calcium release channel, Biophys. J. 101 (9) (2011) 2170–2177. [PubMed: 22067155]

[21]. Shan J, Betzenhauser MJ, Kushnir A, Reiken S, Meli AC, Wronska A, Dura M, Chen BX, Marks AR, Role of chronic ryanodine receptor phosphorylation in heart failure and beta-adrenergic receptor blockade in mice, J. Clin. Invest. 120 (12) (2010) 4375–4387. [PubMed: 21099115]

[22]. Ai X, Curran JW, Shannon TR, Bers DM, Pogwizd SM, Ca2+/calmodulin-dependent protein kinase modulates cardiac ryanodine receptor phosphorylation and sarcoplasmic reticulum Ca2+ leak in heart failure, Circ. Res. 97 (12) (2005) 1314–1322. [PubMed: 16269653]

[23]. Curran J, Hinton MJ, Rios E, Bers DM, Shannon TR, Beta-adrenergic enhancement of sarcoplasmic reticulum calcium leak in cardiac myocytes is mediated by calcium/calmodulin-dependent protein kinase, Circ. Res. 100 (3) (2007) 391–398. [PubMed: 17234966]

[24]. Prosser BL, Ward CW, Lederer WJ, X-ROS signaling: rapid mechano-chemo transduction in heart, Science 333 (6048) (2011) 1440–1445. [PubMed: 21903813]

[25]. Shan J, Xie W, Betzenhauser M, Reiken S, Chen BX, Wronska A, Marks AR, Calcium leak through ryanodine receptors leads to atrial fibrillation in 3 mouse models of catecholaminergic polymorphic ventricular tachycardia, Circ. Res. 111 (6) (2012) 708–717. [PubMed: 22828895]

[26]. Cooper LL, Li W, Lu Y, Centraccio J, Terentyeva R, Koren G, Terentyev D, Redox modification of ryanodine receptors by mitochondria-derived reactive oxygen species contributes to aberrant Ca2+ handling in ageing rabbit hearts, J. Physiol. 591 (23) (2013) 5895–5911. [PubMed: 24042501]

[27]. Erickson JR, Joiner ML, Guan X, Kutschke W, Yang J, Oddis CV, Bartlett RK, Lowe JS, O'Donnell SE, Aykin-Burns N, Zimmerman MC, Zimmerman K, Ham AJ, Weiss RM, Spitz DR, Shea MA, Colbran RJ, Mohler PJ, Anderson ME, A dynamic pathway for calcium-independent activation of CaMKII by methionine oxidation, Cell 133 (3) (2008) 462–474. [PubMed: 18455987]

[28]. Guo T, Zhang T, Mestril R, Bers DM, Ca2+/calmodulin-dependent protein kinase II phosphorylation of ryanodine receptor does affect calcium sparks in mouse ventricular myocytes, Circ. Res. 99 (4) (2006) 398–406. [PubMed: 16840718]

[29]. Curran J, Brown KH, Santiago DJ, Pogwizd S, Bers DM, Shannon TR, Spontaneous Ca waves in ventricular myocytes from failing hearts depend on Ca(2+)-calmodulin-dependent protein kinase II, J. Mol. Cell. Cardiol. 49 (1) (2010) 25–32. [PubMed: 20353795]

[30]. Guo T, Cornea RL, Huke S, Camors E, Yang Y, Picht E, Fruen BR, Bers DM, Kinetics of FKBP12.6 binding to ryanodine receptors in permeabilized cardiac myocytes and effects on Ca sparks, Circ. Res. 106 (11) (2010) 1743–1752. [PubMed: 20431056]

[31]. Zhang H, Makarewich CA, Kubo H, Wang W, Duran JM, Li Y, Berretta RM, Koch WJ, Chen X, Gao E, Valdivia HH, Houser SR, Hyperphosphorylation of the cardiac ryanodine receptor at serine 2808 is not involved in cardiac dysfunction after myocardial infarction, Circ. Res. 110 (6) (2012) 831–840. [PubMed: 22302785]

[32]. Bers DM, Ryanodine receptor S2808 phosphorylation in heart failure: smoking gun or red herring, Circ. Res. 110 (6) (2012) 796–799. [PubMed: 22427320]

[33]. Rebbeck RT, Essawy MM, Nitu FR, Grant BD, Gillispie GD, Thomas DD, Bers DM, Cornea RL, High-throughput screens to discover small-molecule modulators of ryanodine receptor calcium release channels, SLAS Discov. 22 (2) (2017) 176–186. [PubMed: 27760856]

[34]. Rebbeck RT, Singh DP, Janicek KA, Bers DM, Thomas DD, Launikonis BS, Cornea RL, RyR1-targeted drug discovery pipeline integrating FRET-based high-throughput screening and human myofiber dynamic Ca(2+) assays, Sci. Rep. 10 (1) (2020) 1791. [PubMed: 32019969]

[35]. Schaaf TM, Li A, Grant BD, Peterson K, Yuen S, Bawaskar P, Kleinboehl E, Li J, Thomas DD, Gillispie GD, Red-shifted FRET biosensors for high-throughput fluorescence lifetime screening, Biosensors (Basel) 8 (4) (2018).

[36]. Stroik DR, Yuen SL, Janicek KA, Schaaf TM, Li J, Ceholski DK, Hajjar RJ, Cornea RL, Thomas DD, Targeting protein-protein interactions for therapeutic discovery via FRET-based high-throughput screening in living cells, Sci. Rep. 8 (1) (2018) 12560.

[37]. Fruen BR, Bardy JM, Byrem TM, Strasburg GM, Louis CF, Differential Ca(2+) sensitivity of skeletal and cardiac muscle ryanodine receptors in the presence of calmodulin, Am. J. Physiol. Cell Physiol. 279 (3) (2000) C724–C733. [PubMed: 10942723]

[38]. Fruen BR, Black DJ, Bloomquist RA, Bardy JM, Johnson JD, Louis CF, Balog EM, Regulation of the RYR1 and RYR2 Ca2+ release channel isoforms by Ca2 +–insensitive mutants of calmodulin, Biochemistry 42 (9) (2003) 2740–2747. [PubMed: 12614169]

[39]. Cornea RL, Nitu FR, Samso M, Thomas DD, Fruen BR, Mapping the ryanodine receptor FK506-binding protein subunit using fluorescence resonance energy transfer, J. Biol. Chem. 285 (25) (2010) 19219–19226.

[40]. Fruen BR, Balog EM, Schafer J, Nitu FR, Thomas DD, Cornea RL, Direct detection of calmodulin tuning by ryanodine receptor channel targets using a ca(2 +)-sensitive acrylodan-labeled calmodulin, Biochemistry 44 (1) (2005) 278–284. [PubMed: 15628869]

[41]. Schaaf TM, Peterson KC, Grant BD, Bawaskar P, Yuen S, Li J, Muretta JM, Gillispie GD, Thomas DD, High-throughput spectral and lifetime-based FRET screening in living cells to identify small-molecule effectors of SERCA, SLAS Discov. 22 (3) (2017) 262–273. [PubMed: 27899691]

[42]. Schaaf TM, Peterson KC, Grant BD, Thomas DD, Gillispie GD, Spectral unmixing plate reader: high-throughput, high-precision FRET assays in living cells, SLAS Discov. 22 (3) (2017) 250–261. [PubMed: 27879398]

[43]. Guhathakurta P, Prochniewicz E, Grant BD, Peterson KC, Thomas DD, High- throughput screen, using time-resolved FRET, yields actin-binding compounds that modulate actin-myosin structure and function, J. Biol. Chem. 293 (31) (2018) 12288–12298.

[44]. Bassani RA, Bers DM, Rate of diastolic Ca release from the sarcoplasmic reticulum of intact rabbit and rat ventricular myocytes, Biophys. J. 68 (5) (1995) 2015–2022. [PubMed: 7612843]

[45]. Picht E, Zima AV, Blatter LA, Bers DM, SparkMaster: automated calcium spark analysis with Image J, Am. J. Phys. Cell Physiol. 293 (3) (2007) C1073–C1081.

[46]. Hughes JP, Rees S, Kalindjian SB, Philpott KL, Principles of early drug discovery, Br. J. Pharmacol. 162 (6) (2011) 1239–1249. [PubMed: 21091654]

[47]. Hohenegger M, Matyash M, Poussu K, Herrmann-Frank A, Sarkozi S, Lehmann-Horn F, Freissmuth M, Activation of the skeletal muscle ryanodine receptor by suramin and suramin analogs, Mol. Pharmacol. 50 (6) (1996) 1443–1453. [PubMed: 8967964]

[48]. Murayama T, Kurebayashi N, Ishigami-Yuasa M, Mori S, Suzuki Y, Akima R, Ogawa H, Suzuki J, Kanemaru K, Oyamada H, Kiuchi Y, Iino M, Kagechika H, Sakurai T, Efficient high-throughput screening by endoplasmic reticulum Ca(2+) measurement to identify inhibitors of ryanodine receptor Ca(2+)-release channels, Mol. Pharmacol. 94 (1) (2018) 722–730. [PubMed: 29674523]

[49]. Sun J, Yamaguchi N, Xu L, Eu JP, Stamler JS, Meissner G, Regulation of the cardiac muscle ryanodine receptor by O(2) tension and S-nitrosoglutathione, Biochemistry 47 (52) (2008) 13985–13990.

[50]. Aracena P, Sanchez G, Donoso P, Hamilton SL, Hidalgo C, S-glutathionylation decreases Mg2+ inhibition and S-nitrosylation enhances Ca2+ activation of RyR1 channels, J. Biol. Chem. 278 (44) (2003) 42927–42935.

[51]. Feng W, Cherednichenko G, Ward CW, Padilla IT, Cabrales E, Lopez JR, Eltit JM, Allen PD, Pessah IN, Green tea catechins are potent sensitizers of ryanodine receptor type 1 (RyR1), Biochem. Pharmacol. 80 (4) (2010) 512–521. [PubMed: 20471964]

[52]. Feng W, Hwang HS, Kryshtal DO, Yang T, Padilla IT, Tiwary AK, Puschner B, Pessah IN, Knollmann BC, Coordinated regulation of murine cardiomyocyte contractility by nanomolar (−)-epigallocatechin-3-gallate, the major green tea catechin, Mol. Pharmacol. 82 (5) (2012) 993–1000. [PubMed: 22918967]

[53]. Aracena P, Tang W, Hamilton SL, Hidalgo C, Effects of S-glutathionylation and S-nitrosylation on calmodulin binding to triads and FKBP12 binding to type 1 calcium release channels, Antioxid. Redox Signal. 7 (7–8) (2005) 870–881. [PubMed: 15998242]

[54]. Benitez-King G, Huerto-Delgadillo L, Anton-Tay F, Binding of 3H-melatonin to calmodulin, Life Sci. 53 (3) (1993) 201–207. [PubMed: 8321083]

[55]. Sato T, Hirota K, Matsuki A, Zsigmond EK, Rabito SF, Droperidol inhibits tracheal contraction induced by serotonin, histamine or carbachol in Guinea pigs, Can. J. Anaesth. 43 (2) (1996) 172–178. [PubMed: 8825543]

[56]. Li H, Zhao Y, Phillips HI, Qi Y, Lin TY, Sadler PJ, O'Connor PB, Mass spectrometry evidence for cisplatin as a protein cross-linking reagent, Anal. Chem. 83 (13) (2011) 5369–5376. [PubMed: 21591778]

[57]. Mattson MP, Hormesis defined, Ageing Res. Rev. 7 (1) (2008) 1–7. [PubMed: 18162444]

[58]. Chen WP, Hung LM, Hsueh CH, Lai LP, Su MJ, Piceatannol, a derivative of resveratrol, moderately slows I(Na) inactivation and exerts antiarrhythmic action in ischaemia-reperfused rat hearts, Br. J. Pharmacol. 157 (3) (2009) 381–391. [PubMed: 19371352]

[59]. Eisner DA, Trafford AW, Diaz ME, Overend CL, O'Neill SC, The control of Ca release from the cardiac sarcoplasmic reticulum: regulation versus autoregulation, Cardiovasc. Res. 38 (3) (1998) 589–604. [PubMed: 9747428]

[60]. Bers DM, Cardiac sarcoplasmic reticulum calcium leak: basis and roles in cardiac dysfunction, Annu. Rev. Physiol. 76 (2014) 107–127. [PubMed: 24245942]

[61]. Murayama T, Kurebayashi N, Assays for modulators of ryanodine receptor (RyR)/Ca(2+) Release Channel activity for drug discovery for skeletal muscle and heart diseases, Curr. Protoc. Pharmacol. 87 (1) (2019), e71. [PubMed: 31834676]

[62]. Mori S, Iinuma H, Manaka N, Ishigami-Yuasa M, Murayama T, Nishijima Y, Sakurai A, Arai R, Kurebayashi N, Sakurai T, Kagechika H, Structural development of a type-1 ryanodine receptor (RyR1) Ca(2+)-release channel inhibitor guided by endoplasmic reticulum Ca(2+) assay, Eur. J. Med. Chem. 179 (2019) 837–848. [PubMed: 31299492]

[63]. Uchinoumi H, Yano M, Suetomi T, Ono M, Xu X, Tateishi H, Oda T, Okuda S, Doi M, Kobayashi S, Yamamoto T, Ikeda Y, Ohkusa T, Ikemoto N, Matsuzaki M, Catecholaminergic polymorphic ventricular tachycardia is caused by mutation-linked defective conformational regulation of the ryanodine receptor, Circ. Res. 106 (8) (2010) 1413–1424. [PubMed: 20224043]

[64]. Schaaf TM, Kleinboehl E, Yuen SL, Roelike LN, Svensson B, Thompson AR, Cornea RL, Thomas DD, Live-cell cardiac-specific high-throughput screening platform for drug-like molecules that enhance Ca(2+) transport, Cells 9 (5) (2020) 1170. [PubMed: 32397211]

[65]. Gruber SJ, Cornea RL, Li J, Peterson KC, Schaaf TM, Gillispie GD, Dahl R, Zsebo KM, Robia SL, Thomas DD, Discovery of enzyme modulators via high-throughput time-resolved FRET in living cells, J. Biomol. Screen. 19 (2) (2014) 215–222. [PubMed: 24436077]

[66]. Huang X, Liu Y, Wang R, Zhong X, Koop A, Chen SR, Wagenknecht T, Liu Z, Two potential calmodulin binding sequences in the ryanodine receptor contribute to a mobile, intra-subunit calmodulin binding domain, J. Cell Sci. 126 (Pt 19) (2013) 4527–4535. [PubMed: 23868982]

[67]. Wang R, Zhong X, Meng X, Koop A, Tian X, Jones PP, Fruen BR, Wagenknecht T, Liu Z, Chen SR, Localization of the dantrolene-binding sequence near the FK506-binding protein-binding site in the three-dimensional structure of the ryanodine receptor, J. Biol. Chem. 286 (14) (2011) 12202–12212.

[68]. Cashman JR, Ryan D, McKeithan WL, Okolotowicz K, Gomez-Galeno J, Johnson M, Sampson KJ, Kass RS, Pezhouman A, Karagueuzian HS, Mercola M, Antiarrhythmic hit to lead refinement in a dish using patient-derived iPSC cardiomyocytes, J. Med. Chem. 64 (9) (2021) 5384–5403. [PubMed: 33942619]

[69]. Hnatiuk AP, Briganti F, Staudt DW, Mercola M, Human iPSC modeling of heart disease for drug development, Cell Chem. Biol. 28 (3) (2021) 271–282. [PubMed: 33740432]

[70]. Del Prete D, Checler F, Chami M, Ryanodine receptors: physiological function and deregulation in Alzheimer disease, Mol. Neurodegener. 9 (1) (2014) 21. [PubMed: 24902695]

[71]. Abu-Omar N, Das J, Szeto V, Feng ZP, Neuronal ryanodine receptors in development and aging, Mol. Neurobiol. 55 (2) (2018) 1183–1192. [PubMed: 28102470]
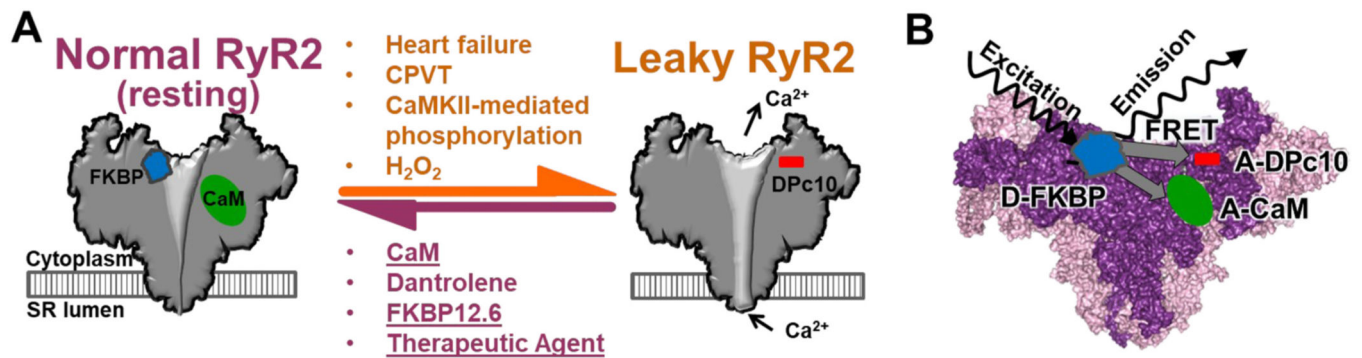
Fig. 1.
Modulators of RyR2 that promote normal (closed) resting channel or pathologically leaky channel, and FRET-based biosensor systems for monitoring modulator binding to RyR2. A) Schematic of the interplay between RyR modulator binding and the healthy vs. pathologically leaky states of the RyR2 in cardiomyocytes. Post-translational modifications that promote RyR2 leak state associated with HF and arrhythmias may reduce binding of RyR stabilizers, FKBP and CaM, and enhance binding of domain peptide, DPc10 [14,15]. Conversely, dantrolene reduces the RyR2 leaky state, increases CaM-RyR2 binding and reduces DPc10-RyR2 binding in cardiomyocytes [14–16]. B) Schematic of FKBP, CaM and DPc10 bound to RyR2 for our FRET assays that use fluorescence lifetime (FLT) measurements of donor (Alexa Fluor 488) attached to FKBP (D-FKBP) in the presence of acceptor (Alexa Fluor 568 or HiLyte Fluor 647) attached to CaM and DPc10, respectively, to gauge shifts in RyR-modulator binding. These assays, previously using fluorescence intensity measurements of FRET in SR membranes and adult cardiomyocytes [14,15,17–20], have been adapted for HTS by exploiting rapid, high-precision FLT measurements of FRET in a plate-reader (PR).
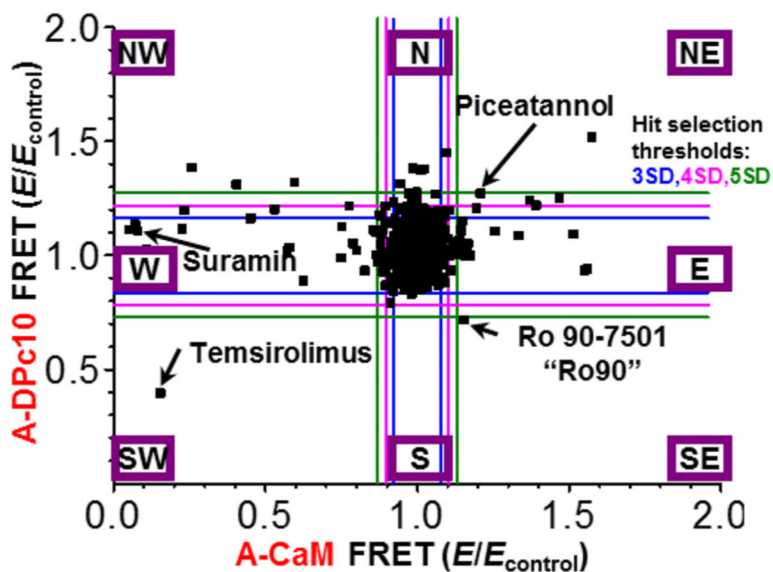
Fig. 2.
Representative orthogonal display of changes in FRET between D-FKBP and A-CaM FRET
or A-DPc10 in a screen of the 1280-compound LOPAC collection. Representative sets
of fluorescence waveforms (primary readout) are shown in Supplementary Fig. 1. FRET
efficiency (E) corresponding to each compound was normalized to the DMSO control
($E_{control}$). Hits were selected outside a 4SD threshold (pink lines) from the mean. For
reference, 3 SD (blue lines) and 5 SD (green lines) are shown. The Hits localize to eight
sectors (each indicated within a purple box) depending on the direction of their effects on
FRET to A-CaM or A-DPc10. (For interpretation of the references to colour in this figure
legend, the reader is referred to the web version of this article.)
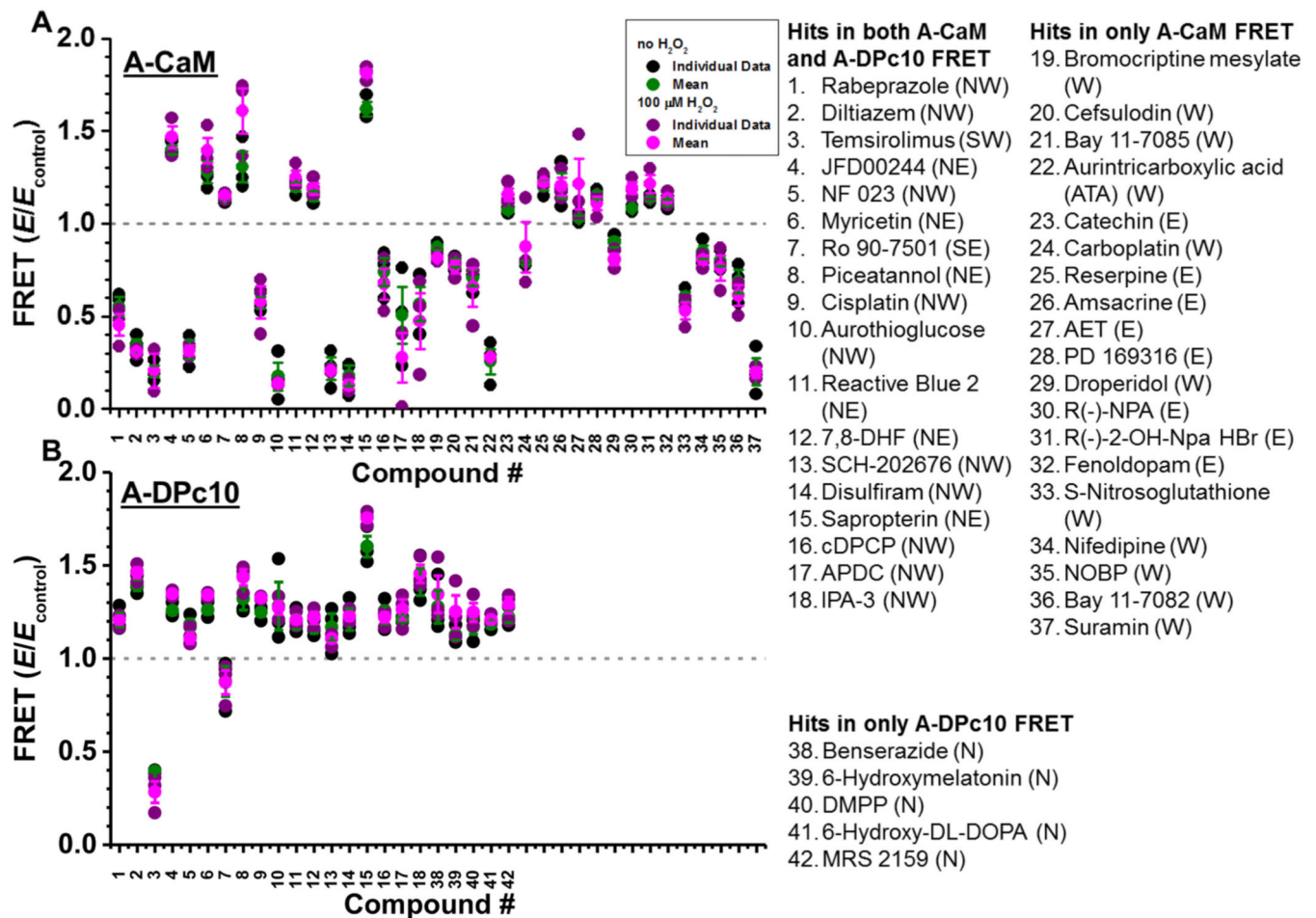
Fig. 3.

Reproducibility of FLT-FRET HTS Hits. Normalized plot of the effects of 10 μM Hit on FRET to A-CaM (A) or A-DPc10 (B) exceeding 4SD in 2 of 3 screens. SR was exposed to no H_2O_2 (black for individual values and green for mean values±SD) and H_2O_2 treatment (purple for individual values and pink for mean values±SD). The first 18 Hits altered both A-CaM and A-DPc10 FRET, Hits 19–37 only altered A-CaM FRET, and Hits 38–42 altered A-DPc10 FRET. These groups were assigned based on the Fig. 2 representation, sectors being indicated in parentheses for each compound. A-CaM $FRET_{control}$ values of SR exposed to no H_2O_2 and plus H_2O_2 treatment were 0.11 ± 0.01 and 0.09 ± 0.01, respectively. A-DPc10 $FRET_{control}$ values of SR exposed to no H_2O_2 and plus H_2O_2 treatment were 0.1 ± 0.02 and 0.11 ± 0.04, respectively. Chemical structures are shown in Supplementary Figs. 2 and 3. (For interpretation of the references to colour in this figure legend, the reader is referred to the web version of this article.)
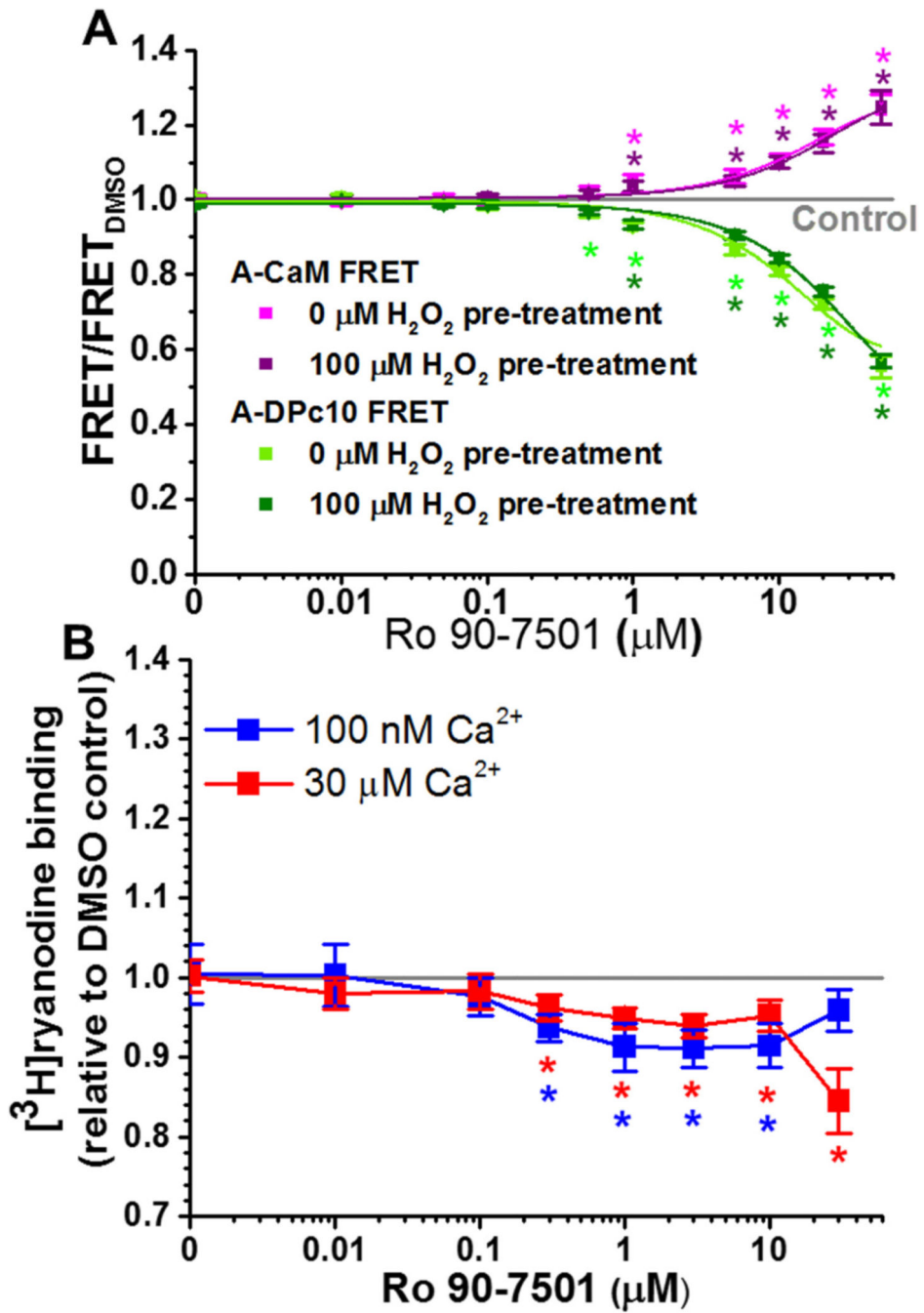
Fig. 4.
Dose-dependent effects of Ro 90–7501. (A) Normalized FLT-FRET response to the indicated Ro 90–7501 concentrations using cardiac SR and A-CaM (purple) or A-DPc10 (green), at 30 nM Ca^{2+} following pre-treatment with no H_2O_2 (light colors), and 100 μM H_2O_2 (dark colors). (B) Response of RyR2 [^{3}H]ryanodine binding to the indicated concentrations of Ro 90–7501, in 100 nM (blue) or 30 μM (red) free Ca^{2+}. Data are normalized relative to the values for no-drug DMSO control (grey line), means ± SEM, n = 3. *P < 0.05 vs. DMSO by 2-sided Student's unpaired t-test. (For interpretation of the

references to colour in this figure legend, the reader is referred to the web version of this article.)
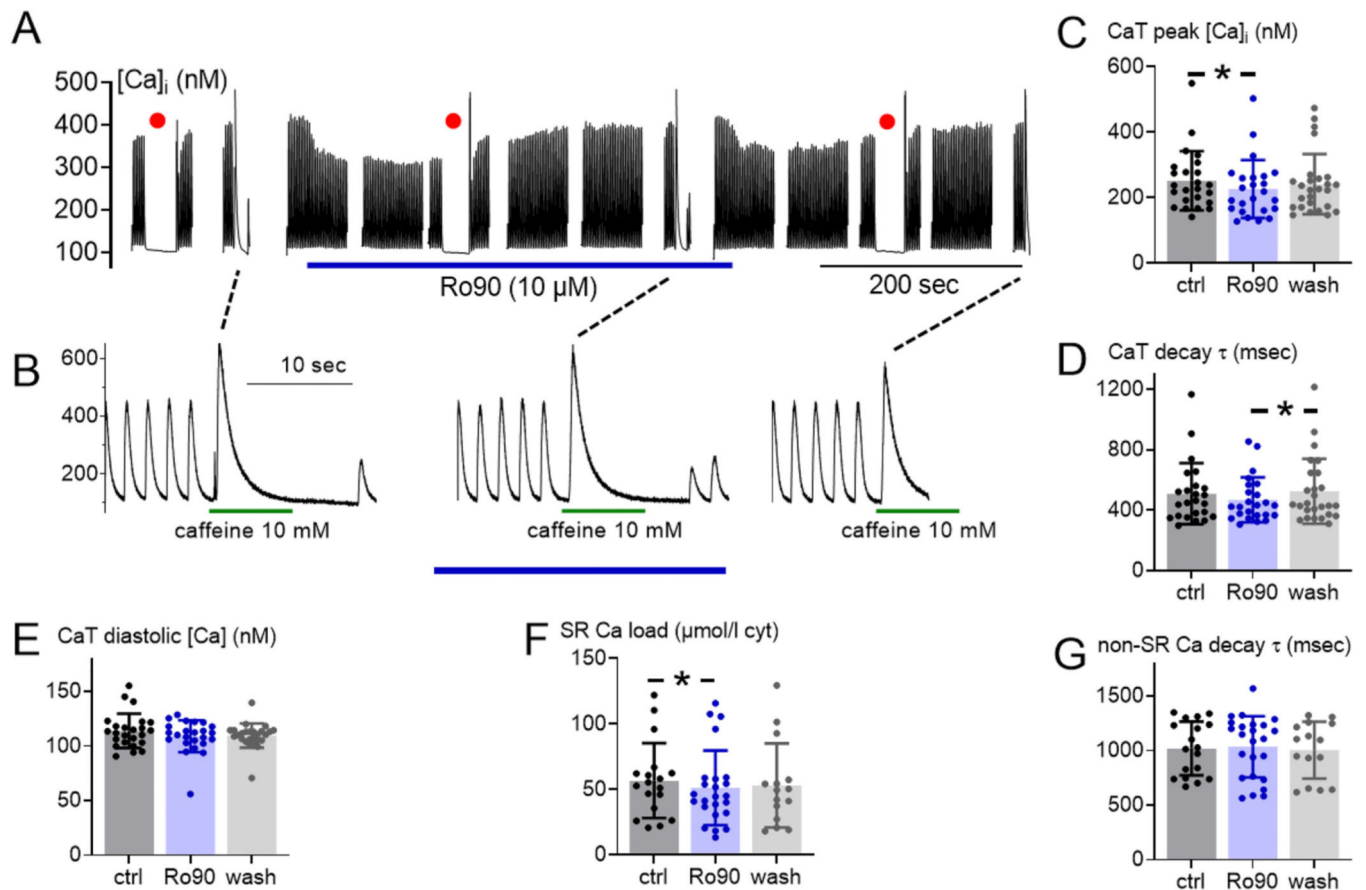
Fig. 5.
Ro 90–7501 does not affect Ca^{2+} handling in normal rabbit myocytes. (A) Time series of a representative experiment with Ro 90–7501 (blue underbar), decimated from $>1 \times 10^6$ data points to a more practical 1×10^4 points. Red dots indicate 30-s rests, showing that the resting fluorescence was stable, thus justifying free $[Ca^{2+}]_i$ pseudo-ratio measurements with resting $[Ca^{2+}]_i$ at baseline assumed to be 100 nM. (B) Detail of the same experiment before, during and after drug contact, each showing the final 10 s of steady state Ca^{2+} transients, followed by 10 mM caffeine (duration 8 s, green underbars) to assay SR Ca^{2+} loading. (C) Peak transient $[Ca^{2+}]_i$, (D) transient $[Ca^{2+}]_i$ decay time constant and (E) residual (diastolic) $[Ca^{2+}]_i$ at the end of each transient, predicted by exponential fitting. (C-E) #cells/#animal (n/N) = 24/10, 24/10, and 26/10 for ctrl, Ro90 and wash, respectively. (F) SR Ca^{2+} loading, represented as total $[Ca^{2+}]$ released to cytosol by caffeine (calculated as in text). (G) Ca^{2+} transient decay time constant measured with caffeine present, representing non-SR Ca^{2+} removal, mainly via Na/Ca exchange. (F and G) n/N = 18/10, 24/10, and 15/10, respectively. $[Ca^{2+}]$ in (C), (E) and (F) shown with one dot per cell, measured via pseudo-ratio relative to the same cell's rest value (red dots in A). *$P < 0.05$ vs. control (ctrl) by 2-sided Student's paired t-test. (For interpretation of the references to colour in this figure legend, the reader is referred to the web version of this article.)
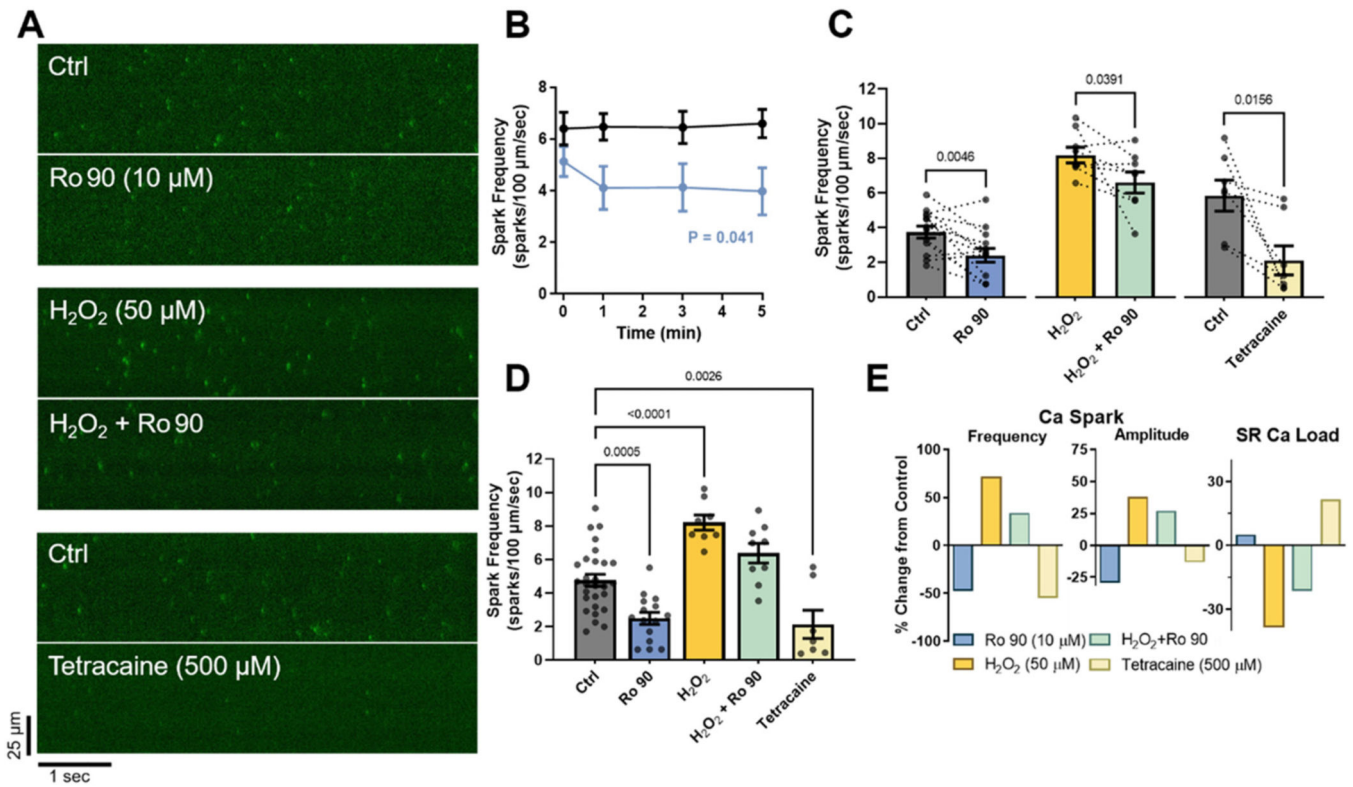
Fig. 6.
Ro 90–7501 effect on Ca^{2+} spark rate in permeabilized rat myocytes. (A) Representative paired line-scan recordings (6 s) of Ca^{2+} sparks response to acute exposure (5 min) to 10 μM Ro 90–7501 or 500 μM tetracaine treatment, as indicated, under either control (Ctrl) conditions or following 50 μM H_2O_2 pretreatment (1 h). Colour display scales span the fluorescence range of Ca^{2+} sparks. (B) Time course of average (±SEM, n/N (# of cells/# of animals) = 7/4 Ctrl, 9/4 Ro 90–7501) Ca^{2+} spark frequencies (CaSpF) with and without 10 μM Ro 90–7501 treatment over 5 min (repeated measures two-way ANOVA with Geisser-Greenhouse correction; Dunnett multiple comparison post-hoc test). (C) Explicit paired comparisons of CaSpF before or after 5 min exposures to either Ro 90 or tetracaine, with or without H_2O_2 pretreatment (Wilcoxon matched-pairs rank tests, n/N = 13/7, 8/3 and 7/3, respectively). (D) CaSpF for individual groups, including unpaired measures, analyzed via one-way ANOVA vs. Ctrl and Dunnett's multiple comparison post-hoc test (n/N = 28/11, 15/7, 8/3, 9/3, 7/3, respectively). (E) Percent change in average Ca^{2+} spark frequency and amplitude relative to respective control averages, and in average SR Ca^{2+} load relative to control average. Statistical analyses were performed using GraphPad Prism 9 software.
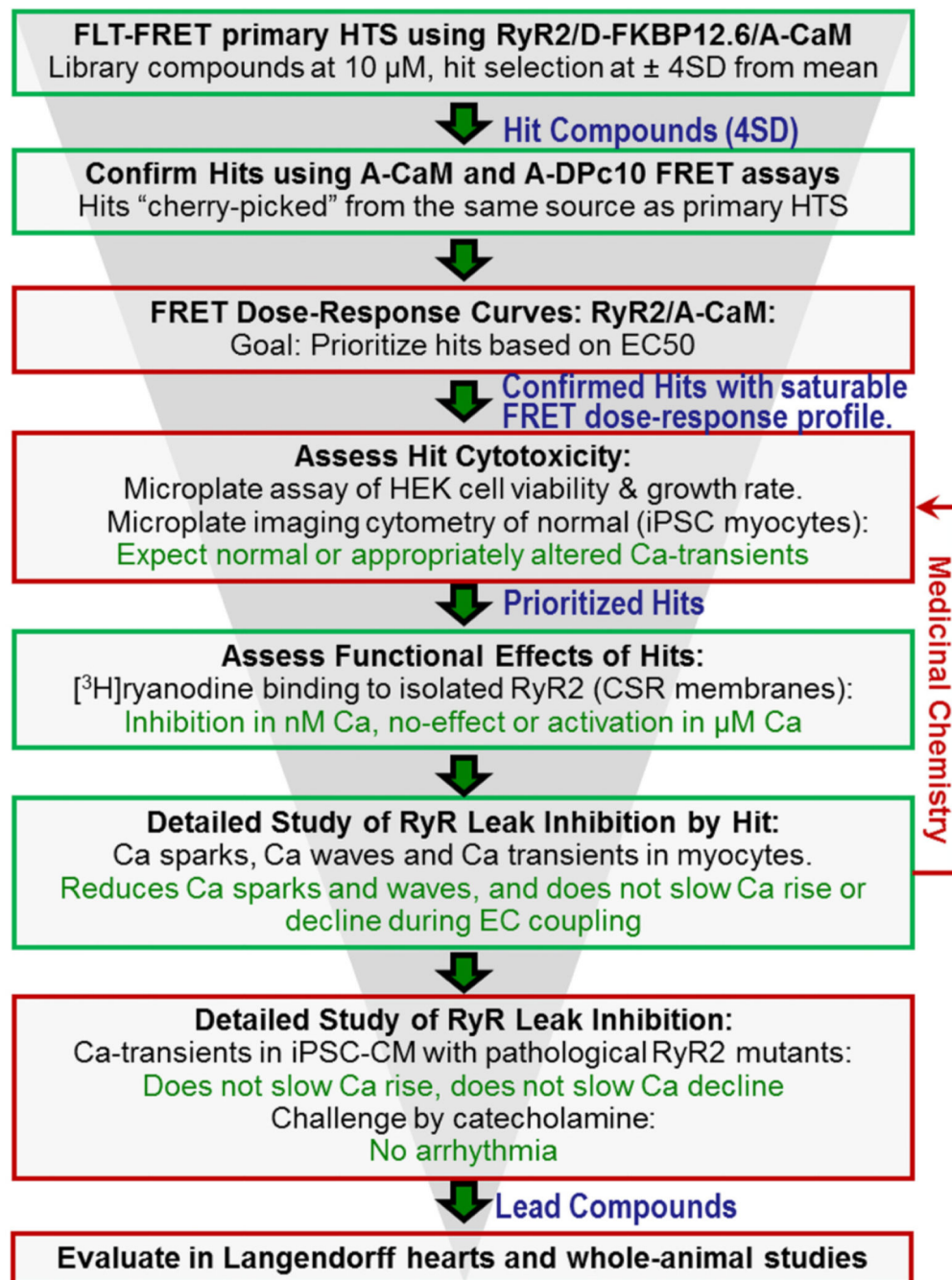
Fig. 7.
RyR2 Drug Discovery Process. Green boxes denote early-stage steps (assays) that are covered in this report. In red, we summarize some of the additional steps that will be necessary to advance compounds in a fully developed drug discovery campaign. (For interpretation of the references to colour in this figure legend, the reader is referred to the web version of this article.)

Table 1

Number (#) of Hits and Hit reproducibility for the 4SD threshold.

A-CaM FRET	No H$_2$O$_2$			H$_2$O$_2$ treatment		
	Plate 1	**Plate 2**	**Plate 3**	**Plate 1**	**Plate 2**	**Plate 3**
# of Hits 20 min	70	24	44	81	51	42
# of Hits 120 min	70	54	54	105	24	60
% of Repeated Hits in 2 plates[a]	52.9	63.0	66.7	37.1	83.3	63.3
% of Repeated Hits in 3 plates[a]	44.3	57.4	57.4	18.1	79.1	31.2
A-DPc10 FRET						
# of Hits 20 min	35	47	25	35	25	31
# of Hits 120 min	26	63	28	28	31	31
% of Repeated Hits in 2 plates[a]	50	36.5	78.6	75.0	71.0	54.8
% of Repeated Hits in 3 plates[a]	46.2	19.0	42.9	50	45.2	45.2

[a]Data for 120 min incubation with compound.